Journal of Materials Chemistry A

Accepted Manuscript

This article can be cited before page numbers have been issued, to do this please use: J. A. Anderson, Z. Zhang, Y. Huang, Z. A. Zafar, S. Imtiaz, R. Razaq, S. Ji and T. Huang, *J. Mater. Chem. A*, 2017, DOI: 10.1039/C7TA00282C.

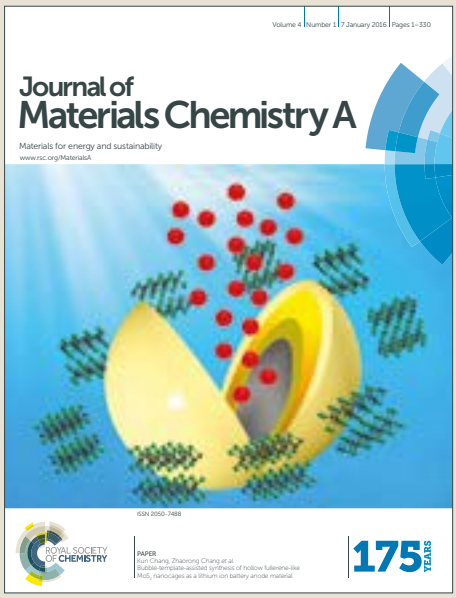

ROYAL SOCIETY OF CHEMISTRY

rsc.li/materials-a

View Article Online
DOI: 10.1039/C7TA00282C

Cathode Materials for Rechargeable Aluminum Batteries: Current Status and Progress

Zahid Ali Zafar[1], Sumair Imtiaz[1], Rameez Razaq[1], Shengnan Ji[1], Taizhong Huang[1], Zhaoliang Zhang[1,*], Yunhui Huang[2,*], James A. Anderson[3,*]

[1] *School of Chemistry and Chemical Engineering, Shandong Provincial Key Laboratory of Fluorine Chemistry and Chemical Materials, University of Jinan, No. 336, West Road of Nan Xinzhuang, Jinan 250022, China*

[2] *State Key Laboratory of Material Processing and Die & Mould Technology, School of Materials Science and Engineering, Huazhong University of Science and Technology, Wuhan, Hubei 430074, China*

[3] *Surface Chemistry and Catalysis Group, Materials and Chemical Engineering, School of Engineering, University of Aberdeen, Aberdeen AB24 3UE, UK*

*Corresponding authors

Zhaoliang Zhang: chm_zhangzl@ujn.edu.cn

Yunhui Huang: huangyh@hust.edu.cn

James A. Anderson: j.anderson@abdn.ac.uk

View Article Online
DOI: 10.1039/C7TA00282C

Abstract

Rechargeable aluminum batteries (RABs) are amongst the most promising of the post-lithium energy storage systems (ESS) with substantially higher specific volumetric capacity (8046 mAh cm^{-3}), higher safety and lower cost. The development of such efficient and low cost ESS is of the essence in order to meet future energy storage demands of modern society. In recent years, a number of research articles have been reported on the evolution of cathode materials for RABs, which makes a critical review timely in order to provide inspiration for future research. This article highlights the cathode materials developed specifically for RABs, in detail, the development of the carbon-based cathode materials, and then that of transition metal oxides (TMOs), sulfides and chloride based cathode materials and then finally, a few other cathode materials are also discussed. Accordingly, future perspectives and opportunities are highlighted.

View Article Online
DOI: 10.1039/C7TA00282C

1. Introduction

In the past few decades, extensive research has been carried out on the development of renewable energy generation and storage systems. Solar, wind and other renewable energy generation technologies are now well developed but all of these technologies are intermittent and require energy storage systems (ESS), such as batteries and supercapacitors [1-3] to buffer between periods of excess production and demand. Unfortunately, less than one percent of the total energy produced from all renewable energy resources can be stored [3, 4]. The rocking-chair LIBs came into existence in the last decade of 20th century and have been proven to be an efficient ESS due to its high energy density and operating voltage [5-7], which are serving from smart portable devices to large energy grid applications. However, the scarcity of lithium resources along with high cost and safety concerns have turned the current research focus towards cost effective, safe, ultrahigh energy density, earth-abundant and environment-friendly ESS [8-15].

RABs are proposed as the next generation ultrahigh volumetric capacity batteries. As a trivalent metal, Al exchanges three electrons during the redox reaction, hence provides approximately four and two fold volumetric capacity (8046 mAh cm^{-3}) [16-18] than the monovalent LIBs (2062 mAh cm^{-3}) [10] and the divalent magnesium-ion batteries (3833 mAh cm^{-3}) [19-22], respectively. Furthermore, Al is the third most abundant element in the earth's crust [23-25] and less reactive and easier handled than Li [18]. A detailed comparison of the characteristics of Al with other metals is summarised in **Table 1**.

Conventionally, RABs work on the principal of intercalation/deintercalation chemistry. More specifically, two interfacial processes take place in the chloroaluminated ionic liquid

View Article Online
DOI: 10.1039/C7TA00282C

(IL) electrolyte based systems. One is between Al metal and the electrolyte where electrochemical deposition and dissolution of Al metal occur at the anode side, the other is between the electrolyte and cathode materials where chloroaluminate anions ($AlCl_4^-$) and trivalent Al^{3+} ions intercalate and deintercalate during the charge/discharge process [26, 27]. However, the development of trivalent RABs is still hindered by the lack of practical and high specific capacity cathode materials. The design principles of cathode materials for RABs have not yet been determined. The current cathode materials reported for RABs are not satisfactory and have suffered many intrinsic problems, such as (a) capacitive behavior without stable discharge voltage plateaus [27-29], (b) very low (less than 0.55 volts) discharge voltages, [27, 30, 31], (c) poor reversibility leading to low coulombic efficiencies [27, 28], (d) low and unstable discharge capacities with sharp decay after few cycles [32, 33], limited cycle life (~100 cycles) [18, 28, 34], structural disintegration and volume expansions due to the intercalation of large sized intercalation products [26, 35, 36]. All of these issues result in the poor electrochemical performance of the current cathode materials and limit the practicability and commercialisation of high energy density RABs.

Very recently, a topical review has been reported by Elia et al. [37] on rechargeable aluminum batteries. In their review, they have summarized the development of several electrochemical aluminum energy storage systems based on aqueous and non-aqueous electrolytes, specifically the attention was paid to the most recent evolution of the electrolytic media characterized by low reactivity towards other cell components. In addition, they have also focused on electrode materials for different aluminum battery systems involving intercalation-deintercalation processes and Al-Sulfur batteries. However, the recent progress on the cathode materials for RABs requires an immediate and

View Article Online
DOI: 10.1039/C7TA00282C

comprehensive review. Thus, this review article has been prepared with a special focus on the current status and progress of the cathode materials for RABs, in order to provide readers with a better understanding of the practical issues and challenges associated with the current cathode materials. The main body of the review is divided into four sub-sections. The first two sections cover the evolution of carbon and transition metal oxide (TMOs) based cathode materials. Later section describes the sulfide and chloride based cathode materials and the last highlights a few other cathode materials which have been reported for RABs. Accordingly, future prospects of cathode materials are suggested in order to address current problems and roadblocks in the commercialisation of low cost, safe and high energy density next generation RAB systems.

2. Current Cathode materials for Rechargeable Aluminum batteries

The role of Al metal in ESS dates back to the 19th century [19, 38-40], but the first secondary aluminum battery was reported in 1973 by Holleck and Giner [41], who demonstrated the use of a chlorine cathode against an Al metal anode in a eutectic molten salt electrolyte composed of $AlCl_3$, KCl and NaCl. However, the further development of cathode materials for RABs was prompted in the last decade, therein different types of materials have been appraised to obtain a practical and low cost post-lithium ESS. All of the reported cathode materials are categorized and discussed in the following sub-sections.

2.1 Carbon based cathode materials

Carbon as energy storage material is being implemented in ESS, due to its exceptional electrochemical properties, high conductivity, low cost and abundance in nature [24, 42, 43]. Porous carbons, activated carbons, graphitic and amorphous carbons have contributed greatly to the development of LIBs, Li-S batteries and other ESS [44-47]. However, in RABs,

View Article Online
DOI: 10.1039/C7TA00282C

the first carbon based cathode was reported in 1988 by Gifford and Palmisani [36], who presented an Al/Graphite battery using a room-temperature ionic liquid (RTIL) electrolyte composed of $AlCl_3$ and 1,2-dimethyl-3-propylimidazolium-chloride (DMPIC) with a molar ratio of 1.5:1. The average operating voltage was 1.7 volts with discharge capacities in the range of 35 to 40 mAh $g^{-1}_{(Graphite)}$ at the current densities of 1-10 mA $g^{-1}_{(Graphite)}$. The battery was run for more than 150 cycles at 100% depth of discharge (DOD). However, the evolution of Cl_2 gas limited further development of this system.

Aside from pure graphite, Rani et al. [28] reported an electrochemically fluorinated natural graphite (FG) as a cathode in a RTIL electrolyte, composed of $AlCl_3$ and 1,3-di-n-butylimidazolium bromide ([bim] [Br]) with a molar ratio of 0.5:1. The as-prepared cathode was made up of semi-ionic C-F bonds and showed a high discharge capacity of 225 mAh g^{-1} for up to 40 cycles. However, the coulombic efficiency was only 75%. Furthermore, there were no obvious charge/discharge plateaus in the charging and discharging curves. Previously, FG has also been reported by Levitin et al. [48] as a cathode material in an organic electrolyte and found that the high degree of fluorination (63%) significantly improved the discharged capacity.

More recently, Jiao's research group [35] developed a low cost and safer RABs by applying a commercial carbon paper as cathode material in a RTIL electrolyte utilizing $AlCl_3$ and 1-ethyl-3-methylimidazolium chloride [EMIm]Cl ($AlCl_3$/[EMIm]Cl=1.3 by mole). The intermediate voltage plateau was calculated at around 1.8 volts which made this system more practical and viable. Moreover, the stainless steel current collector was replaced by molybdenum to avoid potential corrosion reactions of stainless steel in the acidic RTIL electrolyte. The most important finding was the confirmation of the

View Article Online
DOI: 10.1039/C7TA00282C

intercalation/deintercalation of two types of ions, Al^{3+} and chloroaluminate $[Al_xCl_y]^-$ during the charge/discharge process, which introduced the theory of "multi-coordination ion/single ion intercalation and deintercalation". On account of intercalation of comparatively large $[Al_xCl_y]^-$ anions, the volume of the carbon paper was expanded evidently after just 20 cycles, as observable in the TEM and HRTEM images taken before and after the charging **(Fig. 1 a-b).** The Al/graphite paper based battery showed good discharge capacity of 84.55 mAh g^{-1} at the current density of 50 mA g^{-1} up to 50 cycles however, at high current density of 100 mA g^{-1} the obtained capacity was only 70 mAh g^{-1} **(Fig. 1 c-d)**. Although the discharge capacity for the reported battery was low, the cheap carbon paper showed promising aspects in the commercial applications of the RABs. Hence, the first industrialized prototype of Ah-level RABs was demonstrated by the same research group [49], based on the identical cathode material to the earlier report [35]. The battery with stable discharge capacity as high as 1.3 Ah at a current density of 10 mA g^{-1} and discharge voltage plateau in the range of 2 to 1.44 V was able to illuminate a LED lamp for 14 h. Moreover, a series of prototype RABs drove a super mini kart steadily. The interesting feature of this battery is that the waste cycled graphitic cathode material was recycled and converted into few-layer graphene by a facile and eco-friendly electrochemical exfoliation. However, the self-discharge was observed about 7.28 and 5.89% per day for the 1st and 10th day, respectively, which was carried out by charging the battery to 2.3 V followed by resting for 24 h and draining to 0.3 V at 10 mA g^{-1}. In the subsequent cycles, a self-discharge of nearly 6% per day was recorded which is still very high. Furthermore the energy density (36 Wh/kg) was also low in comparison with lead-acid batteries and aqueous LIBs [50]. In addition, the consumption of high cost RTIL electrolyte was quite high

View Article Online
DOI: 10.1039/C7TA00282C

(142.8 mL per Ah), which puts into question the feasibility and industrialization of the proposed RAB prototype. In order to avoid the use of expensive and extremely moisture sensitive RTIL electrolyte, Jiao et al.[51] demonstrated a low cost alkali chloroaluminate ($NaCl\text{-}AlCl_3$) electrolyte for long life rechargeable aluminum battery working at 120°C. This reflects remarkable progress, because the operating temperature for similar batteries using melt salts as electrolyte was impracticably high (~200°C) in the past [52, 53]. The high discharge capacity of 190 mAh g^{-1} was delivered at a current density of 100 mA g^{-1}. Meanwhile, a good cycling performance was obtained at extremely high current density of 4000 mA g^{-1} with a discharged capacity of 60 mAh g^{-1}, maintained up to 5000 cycles and finally, 43 mAh g^{-1} was recorded after 9000 cycles with a coulombic efficiency constantly above 99% **(Fig. 2 a-c)**. In addition, the alkali chaloroaluminate based RAB also exhibited good shelf-life, as only 20% of potential was lost after 3 months of resting. However, the high temperature operation makes this system impracticable and less appealing.

Graphene has been established as a viable choice for energy storage and conversion devices along with biosensors and catalysts [54-63], owing to its good physical, mechanical and electrochemical properties including high specific surface area and excellent thermal and electrical conductivity [64-66]. In particular, 3D-graphene based materials have appeared as a practical cathode and anode materials for ESS [63, 67-70]. Recently a RAB employing 3D-Graphene foam (3D-GF) as a cathode with stable and high voltage, ultra-high cycle life and ultrafast charging/discharging was discovered by Dai's group [26], representing a major breakthrough in the field of RABs with unprecedented results. The RAB utilizing RTIL electrolyte showed a relatively high specific capacity of 70 mAh $g^{-1}$with a coulombic efficiency of over 98%. This was the first RAB with high and well-defined discharge

View Article Online
DOI: 10.1039/C7TA00282C

plateau of 2 volts. The 3D-GF material with a flexible structure showed very stable cycle life of more than 7500 cycles without reducing capacity and providing an excellent rate capability even at a very high current density of 6000 mA g^{-1}. Significantly, the battery showed a very fast charging time of nearly 1 minute at an extremely high current density of 4000 mA g^{-1} **(Fig. 3 a-d)**. Dai's work contributed greatly in the development of RABs as many key factors were discussed. For instance, (i) the optimized molar ratio of $AlCl_3$ to [EMim]Cl was determined as 1.3; (ii) the high water content (>7500 to 10000 ppm) results in a low coulombic efficiency and H_2 evolution, so a controlled level of water was found to be 500 to 700 ppm in a RTIL electrolyte, and (iii) the charge cut-off voltage was dictated to be 2.45V or less due to electrolyte side reactions at high voltage.

More recently, Dai's group also reported a monolithic 3D graphitic foam (3D-GrF) [71] containing aligned few-layered graphene sheets and low density of defects or oxygen groups as a follow on to their previous work [26]. A new strategy was implemented by the research team in order to reduce the diffusion path for the $[Al_xCl_y]^-$ to obtain high rate capability. The graphene sheets of 3D-GrF were tailored perpendicular to the current collector so that the electrolyte can readily diffuse into the sheets and ultrafast intercalation/deintercalation of $[Al_xCl_y]^-$ could be achieved. The RABs with this configuration resulted in very promising electrochemical performance, exhibiting a high discharge voltage plateau of 1.8 V, a discharge capacity of 60 mAh g^{-1} at an extremely high current density of 12000 mA g^{-1} and a coulombic efficiency of almost 100% with about 100% capacity retention over 4000 cycles.

Inspired by Dai's work [26], Yang et al. [72] applied a unique approach to develope interconnected 3D graphene mesh network (3D-GMN) using folded Ni mesh-assisted CVD

View Article Online
DOI: 10.1039/C7TA00282C

method. The structural parameters of 3D-GMN were optimized by tuning the Ni mesh period and electroplating time. It was found that by increasing the density of 3D-GMN, the electrical conductivity was improved compared to 3D-GF. Furthermore, when 3D-GMN was applied as a cathode in a RAB, it exhibited a fairly high capacity of 57 mAh g^{-1} at an high C-rate of 40 (3000 mA g^{-1}) and excellent capacity retention of 97.5% up to 200 cycles**.**

It should be noted that all 3D-Graphene based materials reported for RABs have shown excellent electrochemical performances. However, they demonstrated rather limited discharge capacities in the range of 60 to 66 mAh g^{-1}, which are not satisfactory for practical applications. In order to improve the specific discharge capacities, a novel strategy was introduced by Yu et al. [73], who prepared graphene nanoribbons on highly porous 3D-graphene (GNHPG) foam by plasma-etching, which provided extra spaces and short diffusion paths for the intercalation/deintercalation of $AlCl_4^-$ anions throughout the 3D-graphene foam. The as-prepared GNHPG material showed exceptionally high electrochemical performance for RABs. The discharge capacity was doubled (123 mAh g^{-1}) compared to the 3D-graphene foams (~60 mAh g^{-1}) at high current density of 5000 mA g^{-1} while maintaining a high coulombic efficiency of 98%. Furthermore, the GNHPG not only enhanced the discharged capacity but an unprecedentedly high cycle life of 10000 cycles was also obtained without any capacity decay **(Fig. 4 a)**. The Al/GNHPG battery as well demonstrated high rate capability at different current densities from 2000 to 8000 mA g^{-1}. Another important feature of GNHPG based rechargeable aluminum battery was its

View Article Online
DOI: 10.1039/C7TA00282C

excellent electrochemical performance at different temperature ranges from 0 to 80^{o}C **(Fig. 4 b-c)**.

The carbon based cathode materials have contributed greatly by showing excellent electrochemical performances in terms of better cycle stability, high rate capability and high cell voltage for the RABs. FG has shown good capacity but short cycle life with low average voltage plateau. The commercial carbon paper has proved to be a high working voltage cathode material in RTIL electrolyte but suffered from structural disintegration, volume expansion and high self-discharge rates. Whereas, in alkali chloroaluminate melt electrolyte it has demonstrated good electrochemical performance but high operating temperature curbed its practicability. In contrast to these, 3D carbons (3D-GF, 3D-GrF, 3D-GMN and GNHPG) exhibited excellent cycling, ultrafast charging/discharging and high rate-capability along with high voltage. The superior electrochemical performance of these materials is enlightened by Lee et al. [74] and Jung et al. [75], who elucidated that the open structured 3D configurations of graphitic foam plays a vital role in the ultrafast charging and discharging. In addition, Wu et al. [76] confirmed the geometry and fast diffusion of $[Al_xCl_y^-]$ anions in the graphite by first principle calculations. However, the capacity was limited to 60 mAh g^{-1} in these carbon based cathode materials except for GNHPF which showed relativity high and stable discharge capacity of 123 mAh g^{-1}. The electrochemical performance of these carbon based cathode materials is mainly due to the intercalation/deintercalation of monovalent chloroaluminate anions rather than trivalent Al^{3+} cations [77]. The monovalent chemistry has placed limitations in the achievement of high capacity RABs, so in order to improve the capacity without reducing the electrochemical

View Article Online
DOI: 10.1039/C7TA00282C

performance, a carbon-based cathode material which encourages trivalent reaction is highly requisite.

2.2 Transition metal oxide (TMOs) based cathode materials

Transition metal oxides (TMOs), in contrast to carbon based materials, have also been used as cathode materials for rechargeable batteries because they provide enough space for intercalation/deintercalation during cycling [78, 79]. Apart from batteries, these materials have performed efficiently in photocatalysis, dye-sensitized solar cells and photoelectrochemistry, owing to the various materials advantages such as surface area and short solid state diffusion paths [80-82]. Since RABs are multivalent-ion batteries, TMOs could be good candidates for cathode materials, as they can accommodate more electrons because of their multivalent nature.

The first report on the use of TMOs in RABs was presented by Paranthaman et al. [83]. They applied λ-Mn_2O_4 as a cathode material in $AlCl_3$/[EMIm]Cl electrolyte with a molar ratio of 2:1. The Al/λ-Mn_2O_4 battery system showed high discharge capacity of 400 mAh g^{-1} and energy density of 1060 Wh/kg compared to LiC_6-Mn_2O_4 system with discharge capacity and energy density of only 106 mAh $g^{-1}$and 424 Wh/kg, respectively. The RAB retained 50% of its initial capacity after 50 cycles.

V_2O_5 has been widely employed in rechargeable batteries[84, 85]. However, the slow diffusion and rigid fixing of Al^{3+} ions between the V_2O_5 interlayers are key concerns of its use in multivalent aluminum batteries. To overcome this issue, Jayaprakash et al. [27] synthesized uniform V_2O_5 nanowires by a facile hydrothermal method **(Fig. 5 a)**, and implemented it as a cathode in a RTIL electrolyte with the molar ratio of 1.1:1. A high discharge capacity (305 mAh g^{-1}) was obtained on its first cycle **(Fig. 5 b)**, and retained up

View Article Online
DOI: 10.1039/C7TA00282C

to 273 mAh g^{-1}after 20 cycles. However, the coulombic efficiency was poor, in addition a practical working voltage could not be maintained. The root cause of the poor performance of this battery was investigated by Reed et al. [86]. They found that the V_2O_5 cathode was electrochemically inactive and the battery-like performance was principally associated with the chromium and iron presented in the stainless steel current collector. These metals were gradually deposited on the anode side of the separator followed by dendrite formation, which consequently failed the battery after 20 cycles. To further elucidate the reactivity of V_2O_5 towards Al in RTIL electrolyte, Wang et al. [30] developed a Ni foam supported binder-free Ni-V_2O_5 cathode and proved that the V_2O_5 was reactive towards Al metal in acidic RTIL electrolyte. They also compared the electrochemical performance of the binder-free Ni-V_2O_5 cathode with PVDF and PTFE binder supported V_2O_5 cathodes and found that the binder-free cathode showed much higher capacity than the binder-assisted cathodes. Moreover, the direct synthesis of the V_2O_5 particles on the Ni foam improved the electrical contact and also provided fast diffusion pathways for Al ions.

Recently, Gu et al. [77] demonstrated the reversible storage of Al^{3+} cations in the V_2O_5 nanowires. The electrochemical activity of V_2O_5 nanowires was observed against the Al metal and two-phase transition reactions were suggested. It was concluded that Al^{3+} cations could be intercalated reversibly into the metal oxide by the intercalation and phase-transition reactions. In addition, formation of amorphous layers on the edges of nanowires was observed due to the intercalation of Al^{3+} which reduced the V^{5+} state. Further, the composite of carbon and amorphous V_2O_5 was studied by Chiku et al. [18]. The maximum discharge capacity of over 200 mAh g^{-1} was obtained for the first cycle. XPS analyses after discharging and the subsequent charging showed the evidence for the occurrence of the

View Article Online
DOI: 10.1039/C7TA00282C

redox changes of the vanadium ion in the V_2O_5/C active material during discharging and charging. Recently, González et al. [87] studied the reversible intercalation of Al ions into orthorhombic V_2O_5 xerogel in 1 M $AlCl_3$ aqueous electrolyte instead of RTIL electrolyte. When tested in a three electrode configuration cell, the as-prepared materials showed good reversible capacity of 120 mAh g^{-1} at a current density of 60 mA g^{-1}. However, the water and protons were also intercalated into V_2O_5 by means of chemical reactions or ion exchange besides the electrochemical intercalation of Al ions. The use of aqueous electrolytes for the multivalent Al batteries is very promising, but the reported battery system here exhibitted poor coulombic efficiency and limited cycle life.

The tunneled-structured VO_2 nanorods, which is considered to be a highly reversible and stable cathode material for LIBs [88-90], was investigated by Wang et al. [29] as potential cathode material for RABs. The as-synthesized VO_2 nanorods **(Fig. 5 c)**, with dimensions of 60-100 nm in width and 1 micrometer in length and SSA of 37 m^2 g^{-1}, exhibited a very stable electrochemical performance in the RTIL electrolyte composed of $AlCl_3$ and 1-butyl-3-methylimidazolium chloride ([BMIm]Cl) in a 1:1 molar ratio. The benzyl sulfoxide (0.5 wt%.) was added to assist corrosion resistance because RTIL electrolytes have a corrosive nature and could affect the battery performance by corroding the stainless steel current collector and coin cell shells. The initial capacity was 165 mAh g^{-1} at the current density of 50 mA g^{-1} and retained up to 116 mAh g^{-1} after 100 cycles **(Fig. 5 d)**. However, the trapping of intercalation products inside the VO_2 tunnels might occur as suggested by the over coulombic efficiency.

Anatase TiO_2 nanotube-arrays (TiO_2-NTAs) were reported as a cathode material for RABs in an aqueous $AlCl_3$ electrolyte by Liu et al. [34]. The obtained results confirmed the

View Article Online
DOI: 10.1039/C7TA00282C

reversible intercalation/deintercalation of Al^{3+} cations into TiO_2-NTAs due to the small ionic radius of Al^{3+} (53.5 pm). The unique structure of the as-prepared TiO_2-NTAs was supportive for both the fast transport of electrons and the short ion diffusion paths. However, the electrochemical performance of anatase TiO_2-NTAs might suffer from the formation of Al oxidative layers on Al anode, other corrosion products and parasitic hydrogen evolution in aqueous systems that hinder redox reactions and lower the cell potential [48, 91]. Subsequently, Liu et al. [82] found that Cl^- ions takes part in the electrochemical insertion/extraction process of Al^{3+} in TiO_2-NTAs. Sang et al. [92] further reported that in aqueous RABs, both H^+ and Al^{3+} have electrochemical activity towards TiO_2-NTAs. However, H^+ takes part in the surface hydroxylation of TiO_2-NTAs and thus a suitable pH value (~3) for $AlCl_3$ based aqueous electrolyte is requisite to minimize the effect of H^+.

TMOs are suggested as practical cathode materials for multivalent ion batteries due to the variable valence and good stability of transition metals. The reported TMOs (V_2O_5, V_2O and TiO_2) in RABs, have presented high capacity than the carbon based cathode materials but the cycle life, coulombic efficiency and cell voltage were compromised. Unlike monovalent lithium, the strong coulombic effect induced by the trivalent Al cations makes its electrochemical intercalation into a host crystal structure very challenging. Therefore, the transition metal oxides, i.e., oxide anionic frameworks, may not be the ideal hosts for RABs [93].

2.3 Sulfide and Chloride based cathode materials

Sulfide and chloride based materials have been utilized successfully in LIBs and supercapacitors, due to their high theoretical capacities and good conductivity[94, 95]. For

View Article Online
DOI: 10.1039/C7TA00282C

RABs, they were proposed as potentially high capacity cathode materials [19]. Donahue et al. [96] introduced an iron(III) chloride ($FeCl_3$) based RAB utilizing a low-temperature molten salt IL electrolyte induced by mixing $AlCl_3$ and [EMIm]Cl. However, the low utilization of active material ($FeCl_3$) in the IL electrolyte limited the discharged capacities. Furthermore, the self-discharge was also encountered inside the Al/$AlCl_3$ system due to the dissolution of $FeCl_3$ into the IL electrolyte, its transfer towards the Al anode and the subsequent reaction with it.

Vanadium chloride (VCl_3) was investigated by Suto et al. [33] in molten RTIL electrolyte. However, the monovalent reaction was found to take place after a few cycles in the Al/VCl_3 cell, instead of the multivalent reaction between V^{3+} and V^0. It was also found that the dissolution of VCl_3 in the RTIL electrolyte was greatly reduced by the addition of the fluorobenzene (FB), although it did not change the VCl_3 reaction process but improved the capacity retention with cycling. This study demonstrated a way of improving the discharge capacity during charge/discharge cycles by controlling the dissolution of the cathode materials using an electrolyte additive.

Besides iron chloride, iron sulfide (FeS_2) was also reported by Koura [52],. Later on, Mori et al. [31] reported FeS_2 in a RTIL electrolyte as a conversion cathode material for RABs and investigated its reaction mechanism at 55^{o}C. The pristine FeS_2 converted into poorly crystalline FeS and amorphous Al_2S_3 and transformed back to FeS_2 during the charging/discharging process **(Fig. 6 a)**, which is different from the reaction observed in monovalent LIBs. For practical applications, the battery suffered from the low cell voltage and the poor cycle stability due to the dissolution of the sulfides into the chloroaluminate RTIL, as suggested previously [19].

View Article Online
DOI: 10.1039/C7TA00282C

Recently, Wang et al. [97] reported a novel nickel sulfide and graphene mircoflake (Ni_3S_2/Graphene) composite cathode material in a RTIL. The tantalum metal was selected as a current collector because of its stability under the potential range of 0 to 2V against $Al^{3+}/AlCl_4^-$. The RABs was constructed in a pouch cell assembly and showed a comparatively high voltage plateau of nearly 1 V vs. $Al^{3+}/AlCl_4^-$. The cell discharge capacity was as high as ca. 300 mAh g^{-1} for the first few cycles at the current density of 100 mA g^{-1}. However, after a few cycles, it was dropped to 60 mAh g^{-1} and then remained constant till 100 cycles with a coulombic efficiency of 99% **(Fig. 6 b-c)**. It was proposed that the Al^{3+} cations were the main intercalating/deintercalating species in the small tunnels (3 Å) of Ni_3S_2 rather than the larger chloroaluminate anions (5.28 Å [34]). The abrupt drop in capacity could be caused by the destruction of the lattice during the Al^{3+} intercalation/deintercalation process. Furthermore, the phenomenon of self-discharge was also examined by charging the battery to 2 and 1.5 V against the $Al^{3+}/AlCl_4^-$ followed by 12 h at rest position. In both cases the open circuit voltage (OCV) dropped to nearly 1.2 V. It is elucidated that at high voltages some side reactions occurred which caused the self-discharge in the reported RAB utilizing graphene-based hybrid cathode material.

More recently, hexagonal nickel sulfide nanobelts (NiS-nanobelts) were utilized as cathode material for RABs based on $AlCl_3$/[EMIm]Cl RTIL electrolyte by Yu et al. [98]. The special nano-banded structure facilitated the electrolyte immersion and enhanced the Al^{3+} diffusion. The Al/NiS battery showed stable electrochemical performance with the OCV of 1.17 V, the coulombic efficiency of 97.66% for the 100th cycle at a current density of 200 mA g^{-1} and charging /discharging capacities of 106.9 and 104.4 mAh g^{-1}, respectively.

View Article Online
DOI: 10.1039/C7TA00282C

However, the cell voltage plateau was low (1.15 V vs. Al^{3+}/Al) and the cycle life (~100 cycles) was also not satisfactory for practical RABs **(Fig. 6 d-e)**. In addition, the NiS showed the same behavior of self-discharge as graphene supported Ni_3S_2 when charged to high cut-off voltages of 2 and 1.7 V and rested for 12 h, as the OCV descended rapidly to approximately 1.2 V after the charging process completed.

In terms of sulfide other than nickel and ferric, very recently, Want et al. [99] reported 3D-hierarchical copper sulfide (CuS) as a cathode material in RTIL electrolyte for RABs. In the initial charge/discharge cycle a high discharge capacity of nearly 240 mAh g-1 was obtained at the current density of 20 mA g^{-1}. However, it descended shortly after few cycles and then a stable discharge capacity of 90 mA g^{-1} was retained up to 100 cycles. It is worth noticing that the coulombic efficiency remained constantly as high as 100%. Still, the reason behind the rapid decay of capacity in CuS microspheres has not been addressed.

Sulfides and chlorides have presented promising results as cathode materials for RABs, but their dissolution into the electrolyte hampers the development of such materials as practical cathodes. Even though additives were introduced into the electrolyte to control dissolution process, this issue has still not been completely resolved. In order to avoid the dissolution of the sulfides and chlorides into the electrolyte, a detailed investigation of the electrochemical reaction mechanisms and extensive optimization of the cathode materials are required. In particular, the optimization of the cathode morphology and further coating with some conductive polymers or carbon materials may restrict the dissolution of the sulfides and chlorides into the electrolyte and enhance the electrochemical performance of the RABs as practiced in Li-S batteries [100, 101].

2.4 Other types of cathode materials

View Article Online
DOI: 10.1039/C7TA00282C

In addition to carbon, TMOs, sulfide and chloride based cathode materials, other types of cathode materials are also reported for use in RABs. Hudak [102] presented chloroaluminate-doped conducting polymers, polypyrrole and polythiophene as cathode materials in a RTIL electrolyte ($AlCl_3$:[EMIm]Cl molar ratio 2:1). The reported conducting polymers demonstrated discharge capacities between 30 and 100 mAh g^{-1}. In detail, polypyrrole showed an initial discharge capacity of 71 mAh g^{-1} at 0.2C (20 mA g^{-1}) and retained 49 mAh g^{-1} after 100 cycles, whereas polythiophene exhibited more promising results with discharge capacity of nearly 90 mAh g^{-1} with a capacity retention of 80% after 100 cycles at 0.2C (16 mA g^{-1}). It was noted that a remarkable coulombic efficiency of 100% was attained for both polymer based cathodes. However, the dissolution of active materials into the electrolyte reduced the capacities. Furthermore, the discharge voltage profiles for both conducting polymers sharply declined and showed average low discharge voltage, which hindered the future development of conducting polymer based cathodes.

The Chevrel phase is worthy of mention in the development of RABs, which can be envisaged as the pillaring of Mo_6S_8 blocks, where six molybdenum atoms form an octahedron inside a cube of eight sulfur atoms [103]. They possess superconductive, high magnetic, thermoelectric and catalytic properties [104]. The unique crystal structure ensures an exceptionally high mobility of mono and multivalent cations (Li^+, Ni^{2+}, Zn^{2+}, Ca^{2+}, Mg^{2+}) in the host Mo_6S_8 lattice, especially in the presence of the Mo_6 clusters that can easily hold up to four electrons. Furthermore, two types of sites are presented between sulfur cubes to accommodate metal cations [103, 105-107]. The Chevrel phase was firstly reported as cathode material for RABs by Geng et al. [93], who tested aluminum batteries in a mixture of $AlCl_3$ and [BMIm]Cl with a molar ratio of 1.5:1 both at room temperature and at

View Article Online
DOI: 10.1039/C7TA00282C

50°C. At room temperature, the reaction rate was found to be sluggish because of the coarse Mo_6S_8 particles, which resulted in poor coulombic efficiency. On the contrary, at 50°C, the coulombic efficiency was slightly more than 100% however, discharge capacity remained at nearly 75 mAh g^{-1} after 50 cycles **(Fig. 7 a)**. Moreover, good reversibility was observed at different current densities. The SEM image of Mo_6S_8 after 50 cycles showed many cracks in the particle surfaces providing evidence of significant mechanical stress during the intercalation/deintercalation process **(Fig. 7 b)**. The greater than 100% coulombic efficiency suggested that Al ions were slowly trapped in Mo_6S_8 crystals (Intercalation/deintercaation>1). The estimated specific energy was roughly 90 Wh/kg with a nominal cell voltage of 0.5 V.

The open-framework Prussian blue analogues (PBAs) are also very promising cathode materials for interaction/deintercalation of monovalent and multivalent ions because they possess large channels and interstitial A sites **(Fig. 7 c)** [108, 109]. Based on this knowledge, Reed et al. [32] synthesized copper hexacyanoferrate (CuHCF) by a precipitation method. In an organic electrolyte, aluminum trifluoromethane sulfonate (Al triflate) dissolved in diethylene glycol dimethyl ether (diglyme) with a molar ratio of 1:5, CuHCF showed the first discharge capacity of 60 mAh g^{-1}. However, the battery barely accomplished 10 to 15 cycles due to deformation of the crystal structure of CuHCF and anode passivation. The Gaussian calculations suggested that the Al/Diglyme complex was the primary intercalating species rather than free Al^{3+} ions, which kinetically hindered the insertion reaction and probably lowered the electrochemical performance of the system.

Previously, PBAs were shown to present good electrochemical performance and long cycle life with high rate capability for many monovalent and divalent ions (Li^+, Na^+, Mg^{2+})

View Article Online
DOI: 10.1039/C7TA00282C

in aqueous systems [108-111]. The residual zeolitic water within the framework plays a shielding role on the charge of multivalent ions and helps insertions of ions [110]. Based on this assumption, Liu et at. [112] demonstrated PBA-CuHCF in an aqueous electrolyte and obtained improved results compared to previously reported in an organic electrolyte. The electrochemical performance was evaluated in a three electrode cell rather than a two electrode battery system. In detail, CuHCF was applied as the working electrode, graphite as the counter electrode and saturated calomel electrode (SCE) as the reference electrode in 0.5 M $Al_2(SO_4)_3$ aqueous electrolyte. A high specific capacity of 62.9 mAh g^{-1} was obtained at a low current density of 50 mA g^{-1}. However, 46.5 mAh g^{-1} was achieved at a high current density of 400 mAh g^{-1} and retained up to 22.5 mAh g^{-1} after 1000 cycles with 100% coulombic efficiency **(Fig. 7 d)**. The gradual capacity fading was attributed to the dissolution of the cathode material into the acidic aqueous medium.

The cathode materials other than carbons, TMOs, chlorides or sulfides have also shown electrochemical performances for RABs. Those based on polymers and cheverel phase Mo_6S_8 demonstrated high average capacities in the range of 30 to 100 mAh g^{-1} and coulombic efficiencies of 100%. The open framework PBA-CuHCF has proved to be a promising cathode material for aqueous aluminum batteries with high cycle life and excellent coulombic efficiency. However, none of these could be confirmed as high capacity cathode materials for RABs and mostly suffered from low capacities and low average cell voltages, which calls for further development and optimization of the cathode materials and design principals of the cathode materials to achieve practical, high capcity and high energy density RABs.

All of the above-quoted cathode materials for RABs are summarized in **Table. 2**.

View Article Online
DOI: 10.1039/C7TA00282C

Conclusions and future outlook

In this review, the cathode materials implemented in RABs to date have been sumarised, in a manner aimed at highlighting the successes and remaining issues which require attention by current and future researchers and scientists intending to work on RABs.

The key characteristics of all reported cathode materials are described comprehensively along with their electrochemical performances. Those based on carbons (FG, 3D-GF, 3D-GMN and 3D-GrF, transition metal oxides, sulfides and chlorides, and other types of cathode materials, including conducting polymers, open framework PBA-CuHCF and Chevrel phase Mo_6O_8, are reported. Besides these, composite cathode materials such as carbon-V_2O_5 and hazelwoodite Ni_3S_2/graphene are also considered. Among these, graphite-based materials have shown the most promising results for RABs, while others have suffered from numerous problems. For instance, (1) capacitive behavior without stable discharge voltage plateaus, (2) very low discharge voltages, below 0.55 volts, (3) poor reversibility and consequently low coulombic efficiencies, (4) low and unstable discharge capacities with sharp decay after few cycles, (5) limited cycle life (~100 cycles), and (6) structural disintegration and volume expansions due to the intercalation of large sized intercalation products. All of these factors lead to the poor electrochemical performance and hamper the commercialization of high energy density RABs.

In order to achieve practical, low cost and high energy density RABs for EVs and grid storage applications, a potential cathode material should not be subject to any side reactions with electrolytes and other battery components. Moreover, it should be mechanically strong enough to retain its morphology and structure during the intercalation and deintercalation of largely sized $[Al_xCl_y^-]$ anions. Three-dimensional graphene foam (3D-GF & 3D-GrF and

View Article Online
DOI: 10.1039/C7TA00282C

GNHPG) and graphene mesh network 3D-GMN were shown to be the most feasible and stable cathodes, since they demonstrated long cycle life and ultrafast diffusion of $[Al_xCl_y^-]$ anions between the graphene layers during cycling. In particular, 3D-GF and GNHPG showed very excellent cycling and rate-capability performances up to 7500 and 10000 cycles at ultrahigh current densities of 4000 and 5000 mAh g^{-1}, respectively without capacity fading. The open structured 3D configurations of graphitic foam and the fast diffusion of $[Al_xCl_y^-]$ anions played a vital role in the ultrafast charging and discharging in 3D-graphene foams. These reports provide a positive outlook on the future prospects of 3D structured graphitic materials, which could be a viable choice as cathode materials for RABs. Most likely, 3D graphene or 3D graphene-based hybrid materials (GBHMs) could address the previously highlighted limitations of these systems in the near future.

It is hoped this paper will provide readers with a better understanding of issues and challenges faced by present cathode materials for RABs. It is believed that this review can urge more researchers and scientists to seek out novel cathode materials and open up new avenues in the development and commercialization of low cost, safer and high energy density next generation RABs.

Acknowledgments

This work was financially supported by the National Natural Science Foundation of China (No. 21477046, 21277060 and 51361130151), Key Technology R&D Program of Shandong Province (No. 2016ZDJS11A03), Science Development Project of Shandong Province (No.2014GGX104004) and Natural Science Foundation of Shandong Province (No. ZR2015EM044).

View Article Online
DOI: 10.1039/C7TA00282C

References:

1. J. P. Barton and D. G. Infield, *IEEE Trans. Energy Convers.*, 2004, **19**, 441.
2. S. Teleke, M. E. Baran, S. Bhattacharya and A. Q. Huang, *IEEE Trans. Sustain. Energy*, 2010, **1**, 117.
3. Z. Yang, J. Zhang, M. C. W. Kintner-Meyer, X. Lu, D. Choi, J. P. Lemmon and J. Liu, *Chem. Rev.*, 2011, **111**, 3577.
4. B. Dunn, H. Kamath and J. M. Tarascon, *Science*, 2011, **334**, 928.
5. B. Scrosati and J. Garche, *J. Power Sources*, 2010, **195**, 2419.
6. V. Etacheri, R. Marom, R. Elazari, G. Salitra and D. Aurbach, *Energy Environ. Sci.*, 2011, **4**, 3243.
7. J.-M. Tarascon and M. Armand, *Nature*, 2001, **414**, 359.
8. Y. Wang, R. Chen, T. Chen, H. Lv, G. Zhu, L. Ma, C. Wang, Z. Jin and J. Liu, *Energy Storage Materials*, 2016, **4**, 103.
9. V. Palomares, P. Serras, I. Villaluenga, K. B. Hueso, J. Carretero-González and T. Rojo, *Energy Environ. Sci.*, 2012, **5**, 5884.
10. C. B. B. John Muldoon, Thomas Gregory, *Chem. Rev.*, 2014, **114**, 11683.
11. C. Xu, Y. Chen, S. Shi, J. Li, F. Kang and D. Su, Sci. Rep., 2015, **5**, 14120.
12. P. Adelhelm, P. Hartmann, C. L. Bender, M. Busche, C. Eufinger and J. Janek, *Beilstein J. Nanotechnol.*, 2015, **6**, 1016.
13. R. C. Massé, E. Uchaker and G. Cao, *Sci. China Mater.*, 2015, **58**, 715.
14. D. Larcher and J.-M. Tarascon, *Nature Chemistry*, 2014, **7**, 19.
15. A. Ponrouch, C. Frontera, F. Bardé and M. R. Palacín, *Nat. Mater.*, 2015, **15**, 169.

View Article Online
DOI: 10.1039/C7TA00282C

16. M. Chiku, H. Takeda, Y. Yamaguchi, E. Higuchi and H. Inoue, *International Journal of Chemistry*, 2013, **5**, 1.

17. M. P. Paranthaman, H. Liu, X. G. Sun, S. Dai and G. M. Brown, *Advances in Batteries for Medium and Large-Scale Energy Storage*, eds. M. Skyllas-Kazacos and T. M. Lim, Woodhead Publishing, 2015, **13**, 463.

18. M. Chiku, H. Takeda, S. Matsumura, E. Higuchi and H. Inoue, *ACS Appl. Mater. Interfaces*, 2015, **7**, 24385.

19. Q. Li and, N. J. Bjerrum, *J. Power Sources*, 2002, **110**, 1.

20. S. Xia, X.-M. Zhang, K. Huang, Y.-L. Chen and Y.-T. Wu, *Journal of Electroanalytical Chemistry*, 2015, **757**, 167.

21. S. Rasul, S. Suzuki, S. Yamaguchi and M. Miyayama, *Electrochim. Acta*, 2012, **82**, 243.

22. S. Y. Ha, Y. W. Lee, S. W. Woo, B. Koo, J. S. Kim, J. Cho, K. T. Lee and N. S. Choi, *ACS Appl. Mater. Interfaces*, 2014, **6**, 4063.

23. Y.-J. Cho, I.-J. Park, H.-J. Lee and J.-G. Kim, *J. Power Sources*, 2015, **277**, 370.

24. K. H. Wedepohl*, Geochim. Cosmochim. Acta*, 1995, **59**, 1217.

25. A. A. Yaroshevsky, Geochem. Int., 2006, **44**, 48.

26. M. C. Lin, M. Gong, B. Lu, Y. Wu, D. Y. Wang, M. Guan, M. Angell, C. Chen, J. Yang, B. J. Hwang and H. Dai, *Nature*, 2015, **520**, 325.

27. N. Jayaprakash, S. K. Das and L. A. Archer, *Chem. Commun.*, 2011, **47**, 12610.

28. J. V. Rani, V. Kanakaiah, T. Dadmal, M. S. Rao and S. Bhavanarushi, *J. Electrochem. Soc.*, 2013, **160**, A1781.

View Article Online
DOI: 10.1039/C7TA00282C

29. W. Wang, B. Jiang, W. Xiong, H. Sun, Z. Lin, L. Hu, J. Tu, J. Hou, H. Zhu and S. Jiao, Sci. Rep., 2013, **3**, 3383.

30. H. Wang, Y. Bai, S. Chen, X. Luo, C. Wu, F. Wu, J. Lu and K. Amine, *ACS Appl. Mater. Interfaces*, 2015, **7**, 80.

31. T. Mori, Y. Orikasa, K. Nakanishi, C. Kezheng, M. Hattori, T. Ohta and Y. Uchimoto, *J. Power Sources*, 2016, **313**, 9.

32. L. D. Reed, S. N. Ortiz, M. Xiong and E. J. Menke, *Chem. Commun.*, 2015, **51**, 14397.

33. K. Suto, A. Nakata, H. Murayama, T. Hirai, J.-i. Yamaki and Z. Ogumi, *J. Electrochem. Soc.*, 2016, **163**, A742.

34. S. Liu, J. J. Hu, N. F. Yan, G. L. Pan, G. R. Li and X. P. Gao, *Energy Environ. Sci.*, 2012, **5**, 9743.

35. H. Sun, W. Wang, Z. Yu, Y. Yuan, S. Wang and S. Jiao, *Chem. Commun.*, 2015, **51**, 11892.

36. P.R. Gifford and J.B. Palmisano, *J. Electrochem. Soc.*, 1988, **135**, 650.

37. G. A. Elia, K. Marquardt, K. Hoeppner, S. Fantini, R. Lin, E. Knipping, W. Peters, J. F. Drillet, S. Passerini and R. Hahn, *Adv. Mater.*, 2016, DOI: 10.1002/adma.201601357.

38. G. W. Heise, E. A. Schumacher and N. C. Cahoon, *ECS Meeting, New York, **October**, 1948.*

39. L. Bockstie, D. Trevethan and S. Zaromb, *J. Electrochem. Soc.*, 1963, **110**, 267.

40. S. Zaromb, *J. Electrochem. Soc.*, 1962, **109**, 1125.

41. G. L. Holleck and Jose Giner, *J. Electrochem. Soc.,* 1972, **119**, 1161.

View Article Online
DOI: 10.1039/C7TA00282C

42. Z. Li, Y. Huang, L. Yuan, Z. Hao and Y. Huang, *Carbon*, 2015, **92**, 41.

43. D.-W. Wang, Q. Zeng, G. Zhou, L. Yin, F. Li, H.-M. Cheng, I. R. Gentle and G. Q. M. Lu, *J. Mater. Chem. A*, 2013, **1**, 9382.

44. X. Li and B. Wei, *Nano Energy*, 2013, **2**, 159.

45. S. W. Lee, B. M. Gallant, H. R. Byon, P. T. Hammond and Y. Shao-Horn, *Energy Environ. Sci.*, 2011, **4**, 1972.

46. S. Imtiaz, J. Zhang, Z. A. Zafar, S. Ji, T. Huang, J. A. Anderson, Z. Zhang and Y. Huang, *Sci. China Mater.*, 2016, **59**, 389.

47. C. Xu, B. Xu, Y. Gu, Z. Xiong, J. Sun and X. S. Zhao, *Energy Environ. Sci.*, 2013, **6**, 1388.

48. G. Levitin, C. Yarnitzky and S. Licht, *Electrochem. Solid State Lett.*, 2002, **5**, A160.

49. S. Jiao, H. Lei, J. Tu, J. Zhu, J. Wang and X. Mao, *Carbon*, 2016, **109**, 276.

50. W. Tang, Y. Zhu, Y. Hou, L. Liu, Y. Wu, K. P. Loh, H. Zhang and K. Zhu, *Energy Environ. Sci.*, 2013, **6**, 2093.

51. S. Jiao, Y. Song, J. Tu, J. Wang, Y. Liu, H. Jiao, X. Mao, Z. Guo and D. Fray, *J. Mater. Chem. A*, 2016, DOI: 10.1039/c6ta09829k.

52. N. Koura, *J. Electrochem. Soc.*, 1980, **127**, 1529.

53. N. J. B. Qingfeng Li, *J. Power Sources*, 2002, **110**, 1.

54. H. Wang, X. Yuan, G. Zeng, Y. Wu, Y. Liu, Q. Jiang and S. Gu, Adv. Colloid Interface Sci., 2015, **221**, 41.

55. H. Gao and H. Duan, Biosens. Bioelectron., 2014, **65**, 404.

56. W. Yang, M. Ni, X. Ren, Y. Tian, N. Li, Y. Su and X. Zhang, *Current Opinion in Colloid & Interface Science*, 2015, **20**, 416.

View Article Online
DOI: 10.1039/C7TA00282C

57. X. Fan, X. Chen and L. Dai, Curr. Opin. Colloid Interface Sci. *e*, 2015, **20**, 429.

58. L. Ren, K. N. Hui, K. S. Hui, Y. Liu, X. Qi, J. Zhong, Y. Du and J. Yang, Sci. Rep., 2015, **5**, 14229.

59. D. Deng, K. S. Novoselov, Q. Fu, N. Zheng, Z. Tian and X. Bao, *Nat. Nanotechnol.*, 2016, **11**, 218.

60. K. S. Novoselov, V. I. Fal'ko, L. Colombo, P. R. Gellert, M. G. Schwab and K. Kim, *Nature*, 2012, **490**, 192.

61. H. Wang, L.-F. Cui, Y. Yang, H. S. Casalongue, J. T. Robinson, Y. Liang, Y. Cui and H. Dai, J. Am. Chem. Soc., 2010, **132**, 13978.

62. D. Wei and J. Kivioja, *Nanoscale*, 2013, **5**, 10108.

63. X. Cao, Z. Yin and H. Zhang, *Energy Environ. Sci.*, 2014, **7**, 1850.

64. A. Ambrosi, C. K. Chua, N. M. Latiff, A. H. Loo, C. H. Wong, A. Y. Eng, A. Bonanni and M. Pumera, *Chem. Soc. Rev.,* 2016, **45**, 2458.

65. Y. Xu, Z. Lin, X. Zhong, X. Huang, N. O. Weiss, Y. Huang and X. Duan, *Nat. Commun.*, 2014, **5**, 4554.

66. H. Ma, M. Ma, J. Zeng, X. Guo and Y. Ma, *Materials Letters*, 2016, **178**, 181.

67. Y. Tao, X. Xie, W. Lv, D. M. Tang, D. Kong, Z. Huang, H. Nishihara, T. Ishii, B. Li, D. Golberg, F. Kang, T. Kyotani and Q. H. Yang, Sci. Rep., 2013, **3**, 2975.

68. Y. Sun, Q. Wu and G. Shi, *Energy Environ. Sci.*, 2011, **4**, 1113.

69. L. Zhang, F. Zhang, X. Yang, G. Long, Y. Wu, T. Zhang, K. Leng, Y. Huang, Y. Ma, A. Yu and Y. Chen, Sci. Rep., 2013, **3**, 1408.

70. Z. S. Wu, Y. Sun, Y. Z. Tan, S. Yang, X. Feng and K. Mullen, J. Am. Chem. Soc., 2012, **134**, 19532.

View Article Online
DOI: 10.1039/C7TA00282C

71. Y. Wu, M. Gong, M. C. Lin, C. Yuan, M. Angell, L. Huang, D. Y. Wang, X. Zhang, J. Yang, B. J. Hwang and H. Dai, Adv. Mater., 2016, DOI: 10.1002/adma.201602958.

72. G. Y. Yang, L. Chen, P. Jiang, Z. Y. Guo, W. Wang and Z. P. Liu, *RSC Adv.*, 2016, **6**, 47655.

73. X. Yu, B. Wang, D. Gong, Z. Xu and B. Lu, *Adv. Mater.*, 2016, DOI: 10.1002/adma.201604118.

74. S. Lee and J. Cho, Angew. Chem. Int. Ed., 2015, **54**, 9452.

75. S. C. Jung, Y.-J. Kang, D.-J. Yoo, J. W. Choi and Y.-K. Han, *J. Phys. Chem. C*, 2016, **120**, 13384.

76. M. S. Wu, B. Xu, L. Q. Chen and C. Y. Ouyang, *Electrochim. Acta*, 2016, **195**, 158.

77. S. Gu, H. Wang, C. Wu, Y. Bai, H. Li and F. Wu, *Energy Storage Materials*, 2016, **6**, 9.

78. Y. Jiang, M. Hu, D. Zhang, T. Yuan, W. Sun, B. Xu and M. Yan, *Nano Energy*, 2014, **5**, 60.

79. J. Jiang, Y. Li, J. Liu, X. Huang, C. Yuan and X. W. Lou, *Adv. Mater.*, 2012, **24**, 5166.

80. M. Shi, W. Wei, Z. Jiang, H. Han, J. Gao and J. Xie, *RSC Adv.*, 2016, **6**, 25255.

81. R. K. Singh, R. Kumar and D. P. Singh, *RSC Adv.*, 2016, **6**, 64993.

82. Y. Liu, S. Sang, Q. Wu, Z. Lu, K. Liu and H. Liu, *Electrochim. Acta*, 2014, **143**, 340.

83. M. P. Paranthaman, G. M. Brown, X. Sun, J. Nanda, A. Manthiram and A. Manivannan, *218th ECS Meeting Abstracts*, *Las Vegas,* **October**, 2010.

84. Z. Wang, Q. Su and H. Deng, Phys. Chem. Chem. Phys., 2013, **15**, 8705.

85. M. H. Han, E. Gonzalo, G. Singh and T. Rojo, *Energy Environ. Sci.*, 2015, **8**, 81.

View Article Online
DOI: 10.1039/C7TA00282C

86. Reed L. D. and M. E., *J. Electrochem. Soc.*, 2013, **160**, A915.

87. J. R. González, F. Nacimiento, M. Cabello, R. Alcántara, P. Lavela and J. L. Tirado, *RSC Adv.*, 2016, **6**, 62157.

88. D. W. Murphy, P. A. Christian, F. J. DiSalvo, J. N. Carides, and J. V. Waszczak, *J. Electrochem. Soc.*, 1981, **128,** 2053.

89. C. Nethravathi, B. Viswanath, J. Michael and M. Rajamath, *Carbon*, 2012, **50**, 4839.

90. C. Nethravathi, C. R. Rajamathi, M. Rajamathi, U. K. Gautam, X. Wang, D. Golberg and Y. Bando, *ACS Appl. Mater. Interfaces*, 2013, **5**, 2708.

91. M. Mokhtar, M. Z. M. Talib, E. H. Majlan, S. M. Tasirin, W. M. F. W. Ramli, W. R. W. Daud and J. Sahari, J. Ind. Eng. Chem., 2015, **32**, 1.

92. S. Sang, Y. Liu, W. Zhong, K. Liu, H. Liu and Q. Wu, *Electrochim. Acta*, 2016, **187**, 92.

93. L. Geng, G. Lv, X. Xing and J. Guo, Chem. Mater., 2015, **27**, 4926.

94. X. Rui, H. Tan and Q. Yan, *Nanoscale*, 2014, **6**, 9889.

95. X. Xu, W. Liu, Y. Kim and J. Cho, *Nano Today*, 2014, **9**, 604.

96. F. M. Donahue, S. E. Mancini and L. Simonsen, J. Appl. Electrochem., 1992, **22**, 230.

97. S. Wang, Z. Yu, J. Tu, J. Wang, D. Tian, Y. Liu and S. Jiao, *Adv. Energy Mater., 2016, **6**, 1600137.*

98. Z. Yu, Z. Kang, Z. Hu, J. Lu, Z. Zhou and S. Jiao, *Chem. Commun.*, 2016, **52**, 10427.

99. S. Wang, S. Jiao, J. Wang, H.-S. Chen, D. Tian, H. Lei and D.-N. Fang, *ACS Nano*, 2016, DOI: 10.1021/acsnano.6b06446

100. Y. Yang, G. Yu, J. J. Cha, H. Wu, M. Vosgueritchian, Y. Yao, Z. Bao, and Y. Cui, *ACS Nano*, 2011, **5**, 9187.

View Article Online
DOI: 10.1039/C7TA00282C

101. Z. Zhang, H.-K. Jing, S. Liu, G.-R. Li and X.-P. Gao, *J. Mater. Chem. A*, 2015, **3**, 6827.

102. N. S. Hudak, *J. Phys. Chem. C*, 2014, **118**, 5203.

103. M. M. Huie, D. C. Bock, E. S. Takeuchi, A. C. Marschilok and K. J. Takeuchi, Coord. Chem. Rev., 2015, **287**, 15.

104. G. Gershinsky, O. Haik, G. Salitra, J. Grinblat, E. Levi, G. Daniel Nessim, E. Zinigrad and D. Aurbach, J. Solid State Chem., 2012, **188**, 50.

105. E. Levi, A. Mitelman, D. Aurbach and M. Brunelli, Chem. Mater., 2007, **19**, 5131.

106. E. Lancry, E. Levi, A. Mitelman, S. Malovany and D. Aurbach, J. Solid State Chem., 2006, **179**, 1879.

107. E. Levi, G. Gershinsky, D. Aurbach and O. Isnard, Inorg. Chem., 2009, **48**, 8751.

108. M. Pasta, C. D. Wessells, N. Liu, J. Nelson, M. T. McDowell, R. A. Huggins, M. F. Toney and Y. Cui, *Nat. Commun.*, 2014, **5**, 3007.

109. Y. Mizuno, M. Okubo, E. Hosono, T. Kudo, K. Oh-ishi, A. Okazawa, N. Kojima, R. Kurono, S.-i. Nishimura and A. Yamada, *J. Mater. Chem. A*, 2013, **1**, 13055.

110. R. Y. Wang, C. D. Wessells, R. A. Huggins and Y. Cui, Nano Lett., 2013, **13**, 5748.

111. H. Kim, J. Hong, K. Y. Park, H. Kim, S. W. Kim and K. Kang, Chem. Rev., 2014, **114**, 11788.

112. S. Liu, G. L. Pan, G. R. Li and X. P. Gao, *J. Mater. Chem. A*, 2015, **3**, 959.

113. K. Barbalace, *EnvironmentalChemistry.com*, 1995-2016, **http://EnvironmentalChemistry.com/yogi/periodic/**.

114. M. E. Wieser, N. Holden, T. B. Coplen, J. K. Böhlke, M. Berglund, W. A. Brand, P. De Bièvre, M. Gröning, R. D. Loss, J. Meija, T. Hirata, T. Prohaska, R. Schoenberg,

View Article Online
DOI: 10.1039/C7TA00282C

G. O'Connor, T. Walczyk, S. Yoneda and X.-K. Zhu, Pure Appl. Chem., 2013, **85**, 1047.

115. G. Milazzo and S. Caroli, *J. Electrochem. Soc.*, 1978, **125**, 261C.

View Article Online
DOI: 10.1039/C7TA00282C

Figure 1

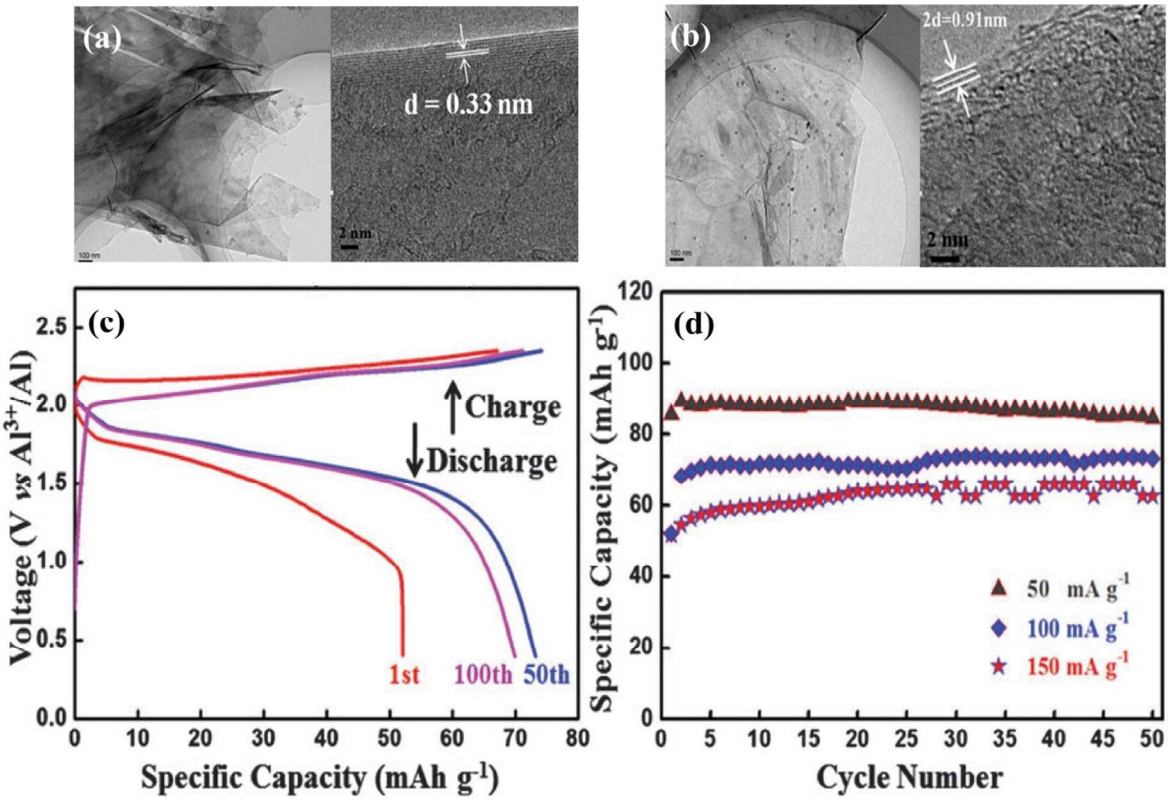

Figure 1 (a) TEM (left) and HRTEM (right) images of Carbon-paper before, and (b) after charging, (c) Al/Carbon-paper battery charge–discharge curves at 100 mA g^{-1} for the 1^{st}, 50^{th} and 100^{th} cycles, and (d) Cycling performances at different current densities over 50

View Article Online
DOI: 10.1039/C7TA00282C

cycles. Reprinted with permission from Ref. [35], Copyright 2015, Royal Society of Chemistry.

Figure 2

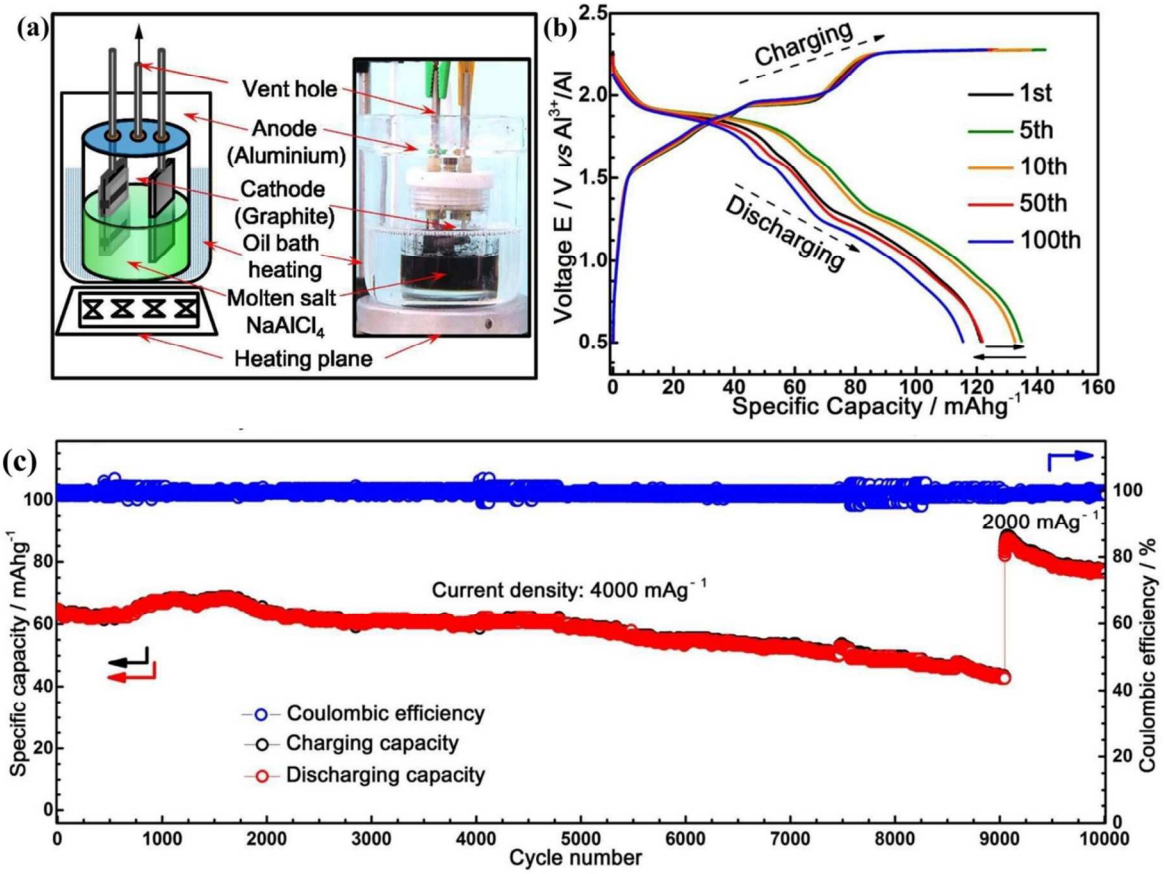

View Article Online
DOI: 10.1039/C7TA00282C

Figure. 2 (a) Depiction of the rechargeable Al/graphite cell, (b) Charge–discharge curves of 1st, 5th, 10th, 50th and 100th cycles at 500mA g^{-1}, and (c) The cycling performance of the Al/carbon paper battery over 9000 cycles at a current density of 4000mA g^{-1} and the extra 1000 cycles at a current density of 2000mA g^{-1}. Reprinted with permission from Ref. [51], Copyright 2016, Royal Society of Chemistry.

Figure 3

View Article Online
DOI: 10.1039/C7TA00282C

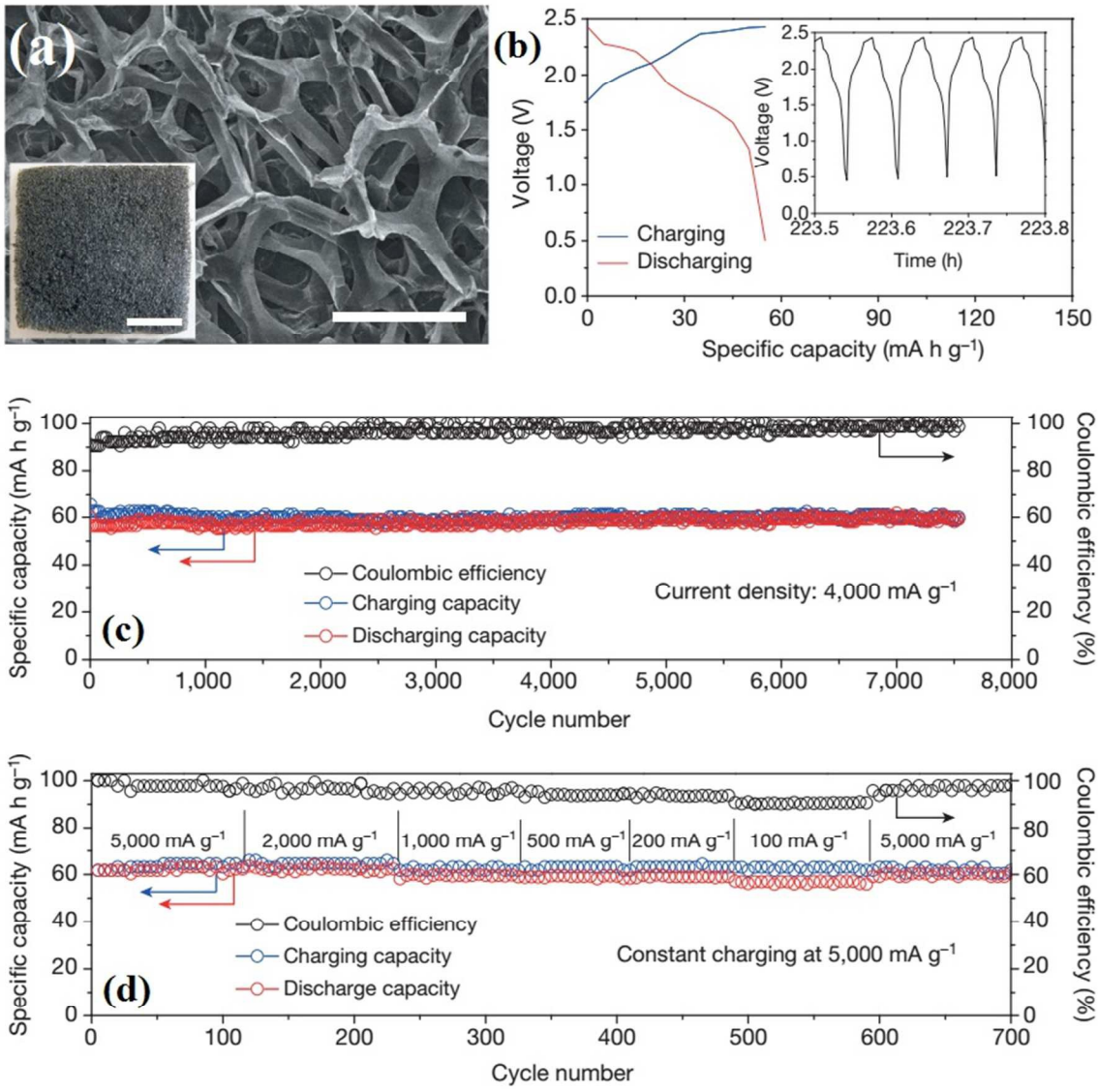

Figure 3 (a) SEM image of a 3D-GF with an open frame structure; scale bar, 300mm. Inset, photograph of 3D-GF; scale bar, 1 cm. (b) Galvanostatic charge and discharge curves of an Al/3D-GF pouch cell at a current density of 4,000 mA g^{-1}. (c) Cycle stability test of an Al/3D-GF pouch cell over 7,500 cycles at a current density of 4,000 mA g^{-1} (d) An Al/3D-GF pouch cell charging at 5,000 mA g^{-1} and discharging at different current densities. Reprinted with permission from Ref. [26], Copyright 2015, Macmillan Publishers.

Figure 4

View Article Online
DOI: 10.1039/C7TA00282C

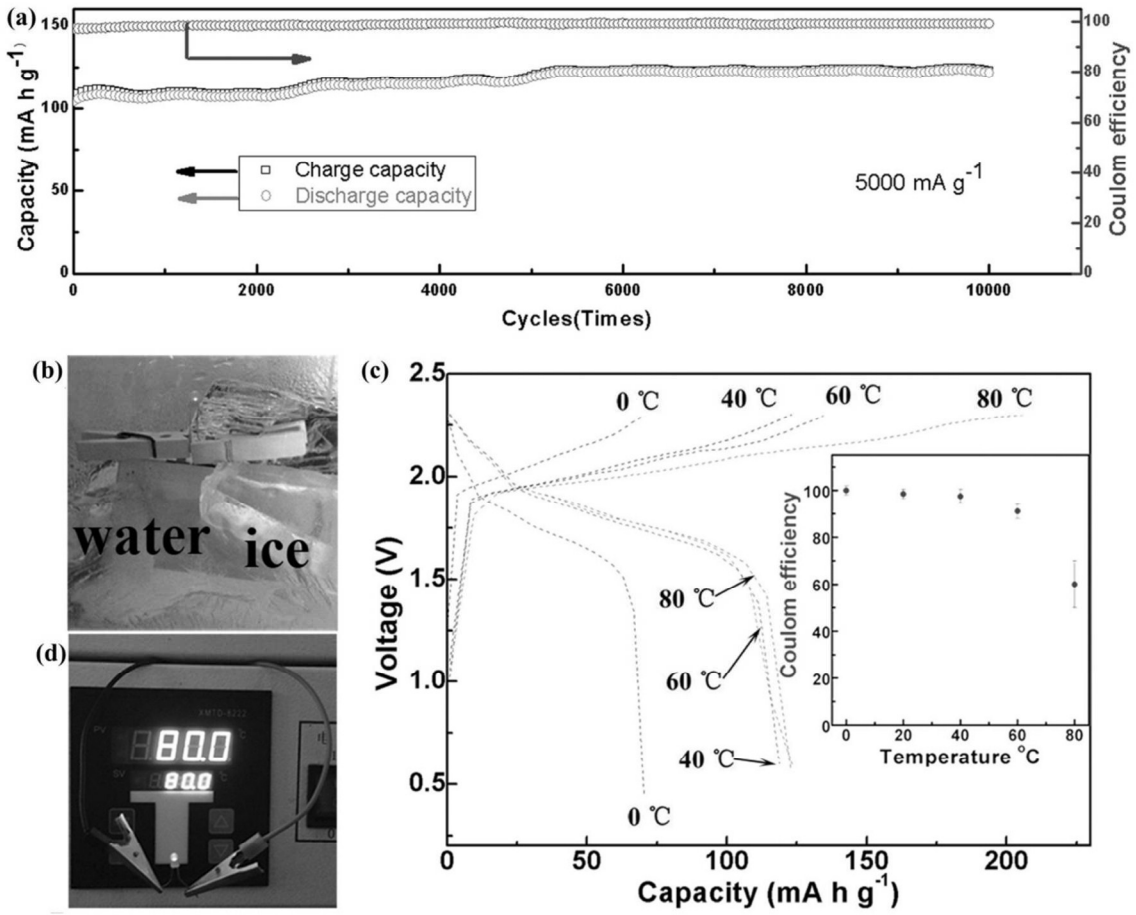

Figure 4 (a) Cycling performance of Al/GNHPG pouch cell at a current density of 5000 mA g^{-1}, (b and c) Al/GNHPG pouch cell working at 0 and 80C, respectively as showing by illumined LED indicator (d) Charge and discharge curves at different temperatures of an Al/GNHPG pouch cell at a current density of 5000 mA g−1. Reprinted with permission from Ref.[73], Copyright 2016, John Wiley and Sons.

Figure 5

View Article Online
DOI: 10.1039/C7TA00282C

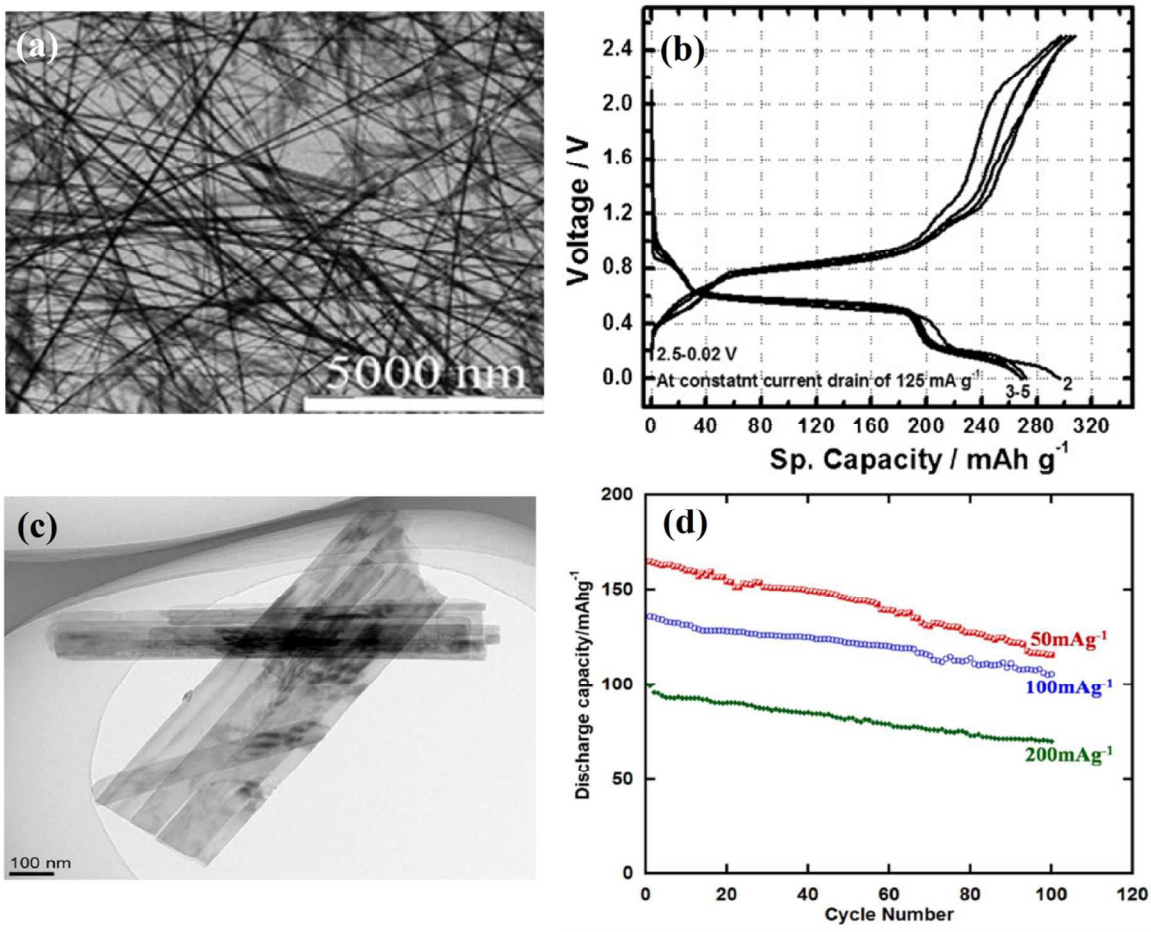

778

779 **Figure 5** (a) TEM image of V_2O_5-nanowires (b) V_2O_5-nanowires based rechargeable Al
780 battery charge/discharge curves for the first few cycles at constant current drain of 125 mA
781 g^{-1}. Reprinted with permission from Ref.[27] Copyright 2011, Royal Society of Chemistry.
782 (c) TEM image of VO_2 and, (d) Cycling performances of VO_2/Al battery under different
783 current densities over 100 cycles. Reprinted with permission from Ref. [29], Copyright 2013,
784 Macmillan Publishers.

785

786

787 **Figure 6**

View Article Online
DOI: 10.1039/C7TA00282C

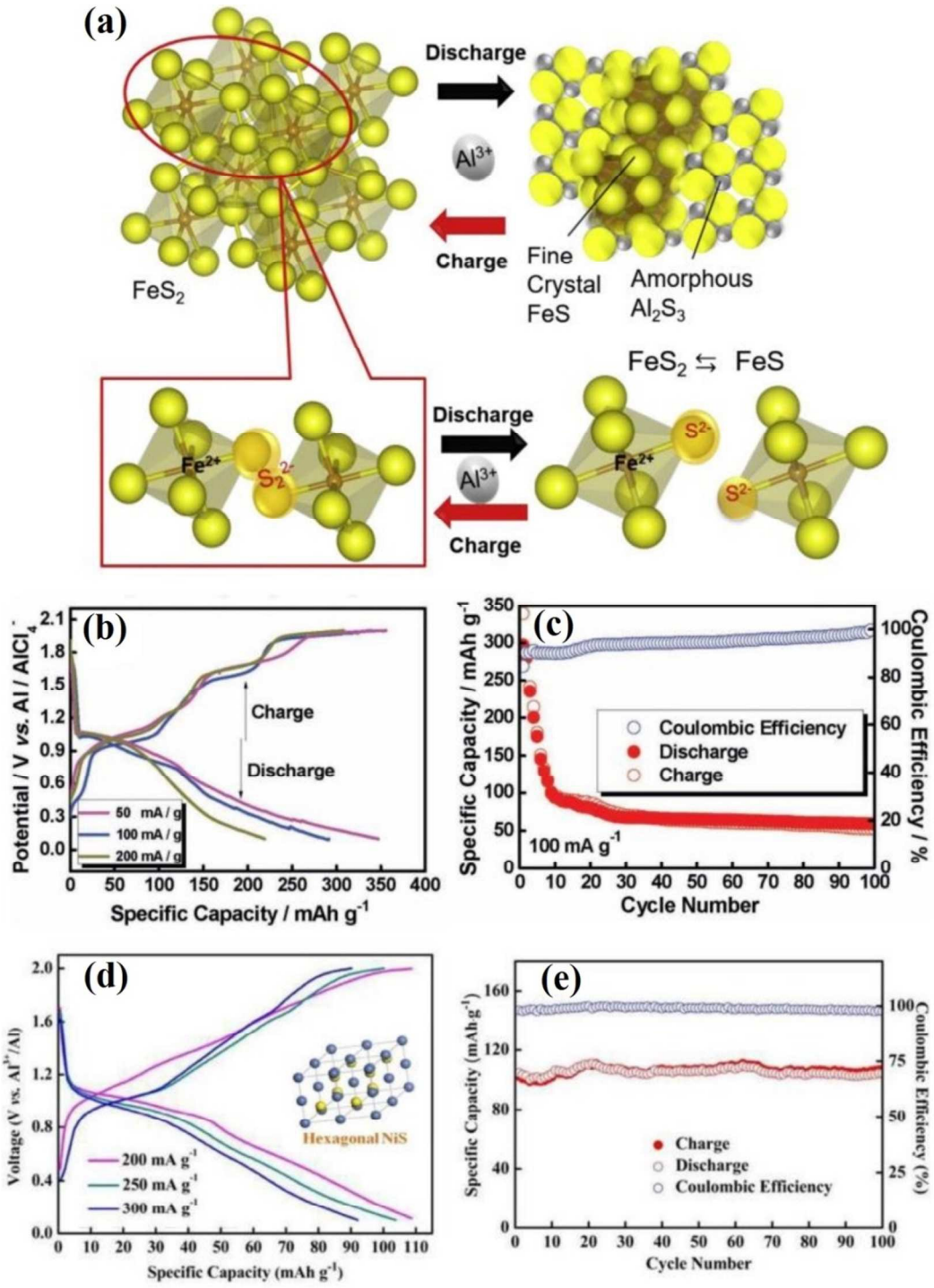

788

789 **Figure 6** (a) Schematic charge-discharge reaction model of FeS_2 with aluminum ions at 55

790 ^{o}C, Reprinted with permission from Ref. [31], Copyright 2016, Elsevier Publishers (b) The

791 charge/discharge curves of Ni_3S_2/Graphene cell for the second cycle at the current densities

View Article Online
DOI: 10.1039/C7TA00282C

of 50, 100, and 200 mA g^{-1}, respectively and (c) Its cycling performance and the coulombic efficiency at a current density of 100 mA g^{-1}. Reprinted with permission from Ref.[97], Copyright 2016, John Wiley and Sons. (d) The cycling performance and the Coulombic efficiency of Al/NiS battery at a current density of 200 mA g^{-1}, inset, Hexagonal structure of NiS and (e) The 10^{th} charge and discharge curves under different current densities. Reprinted with permission from Ref. [98], Copyright 2016, Royal Society of Chemistry.

Figure 7

View Article Online
DOI: 10.1039/C7TA00282C

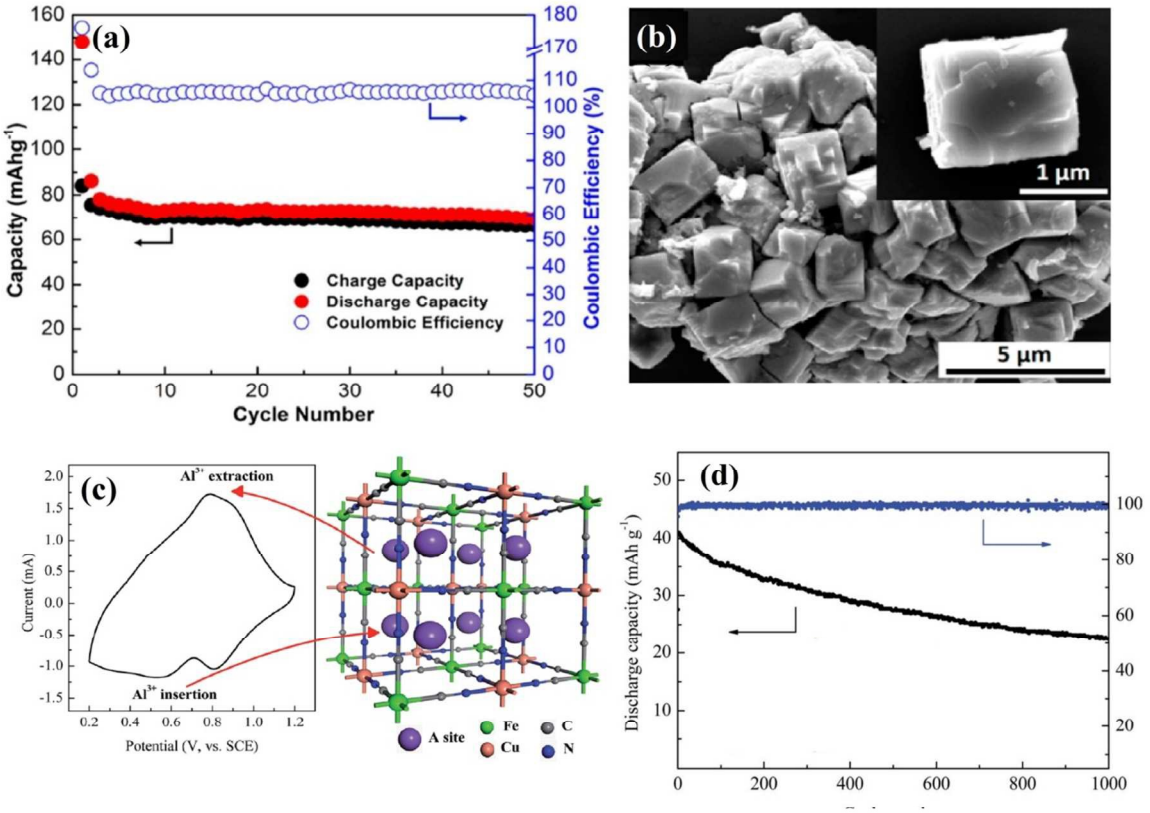

Figure 7 (a) Cycle stability of Al/Mo_6S_8 battery, and (b) SEM image of Chevrel Phase Mo_6S_8, Reprinted with permission from Ref. [93], Copyright 2015, American Chemical Society. (c) Typical CV curve of the CuHCF electrode in aqueous $Al_2(SO_4)_3$ (left) and the schematic positions of Al^{3+} in the interstitial A sites of CuHCF framework (right), (d) The cycle performance of Al/CuHCF based rechargeable Al battery at 400 mA g^{-1} in 0.5 M $Al_2(SO_4)_3$ aqueous solution, inset, the schematic positions of Al^{3+} in CuHCF framework. Reprinted with permission from Ref. [112], Copyright 2015, Royal Society of Chemistry.

Table 1. A comparison of characteristics of aluminum metal with other metals

View Article Online
DOI: 10.1039/C7TA00282C

Category	Na	Ca	Mg	Li	Al	Ref.
Cation radius (Å)	1.02	0.99	0.72	0.76	0.535	113
Atomic weight (g mol^{-1})	22.99	40.07	24.30	6.94	26.98	114
E^o (vs. SHE)	-2.71	-2.84	-2.35	-3.05	-1.67	115
Abundance in Earth's crust (wt%)	2.56	2.94	1.35	0.0022	7.74	25
Capacity (mAh g^{-1}), metal	1165	1337	2205	3861	2980	10
Energy density (mAh ml^{-1})	1128	2073	3833	2262	8046	10
Electrochemical Equivalent (g Ah^{-1})	0.8577	0.7477	0.4534	0.259	0.3355	113

Table 2. Summary of all cathode materials for RABs.

View Article Online
DOI: 10.1039/C7TA00282C

Cathode Material	Publication Year	Initial capacity* (mAh g^{-1})	Capacity retention (mAh g^{-1})	Current density (mA g^{-1})	Mean cell voltage (Volts)	Cycle life	Coulombic efficiency (%)	Electrolyte (Molar ratio)	Ref.
V_2O_5 nano-wires	2011	305	273	125	0.5	20	~88	1.1:1 $AlCl_3$: [EMIm]Cl	27
Anatase TiO_2-NTAs	2012	50	75	4 $mAcm^{-2}$	0.98	13	N/A	1M $AlCl_3$ aqueous solution	34
FG	2013	208	225	60	0.65	40	75	0.5:1 $AlCl_3$: [BIm]Br	28
Polypyrrole	2014	71	49	20	1.42	100	100	1.5:1 $AlCl_3$: [EMIm]Cl	102
Polythiophene	2014	89	71.5	16	1.47	100	100	1.5:1 $AlCl_3$: [EMIm]Cl	102
V_2O_5/C	2015	150	~75	0.05C	<1.0	30	N/A	1:10:5 AlCl3:Dipropylsulfone:Toluene	18
Mo_6S_8#	2015	148	70	6	0.50	50	>100	1:1 $AlCl_3$: [BMIm]Cl	93
PG	2015	60	66	66	~2.0	>200	98.1	1.3:1 $AlCl_3$: [EMIm]Cl	26
3D-GF	2015	~60	60	4000	~2.0	7500	98	1.3:1 $AlCl_3$: [EMIm]Cl	26
CuHCF	2015	41	22.5	400	0.54	1000	100	0.5M $Al_2(SO_4)_3$ aqueous solution	112
Ni-V_2O_5	2015	239	N/A	44.2	0.6	N/A	N/A	1:1 $AlCl_3$: [BMIm]Cl	30
Ni_3S_2@Graphene	2016	235	50	200	~1.0	300	99	1.3:1 $AlCl_3$: [EMIm]Cl	97
3D-GMN	2016	57	57	3000	N/A	200	97.5	1.3:1 $AlCl_3$: [EMIm]Cl	72
NiS	2016	104.7	104.4	200	1.17	100	97.66	1.3:1 $AlCl_3$: [EMIm]Cl	98
CuS	2016	240	90	20	~1	100	100	1.3:1 $AlCl_3$: [EMIm]Cl	99
3D-GrF	2016	60	60	12000	1.8	4000	100	1.3:1 $AlCl_3$: [EMIm]Cl	71
Carbon Paper$	2016	60	43	4000	~1.8-1.2	9000	99	1.63:1 $AlCl_3$: NaCl	51
GNHPG	2016	123	123	5000	~2.0	10000	98	1.3:1 $AlCl_3$: [EMIm]Cl	73

839 #: Electrochemical performance at 50 °C
840 $: Electrochemical performance at 120 °C

View Article Online
DOI: 10.1039/C7TA00282C

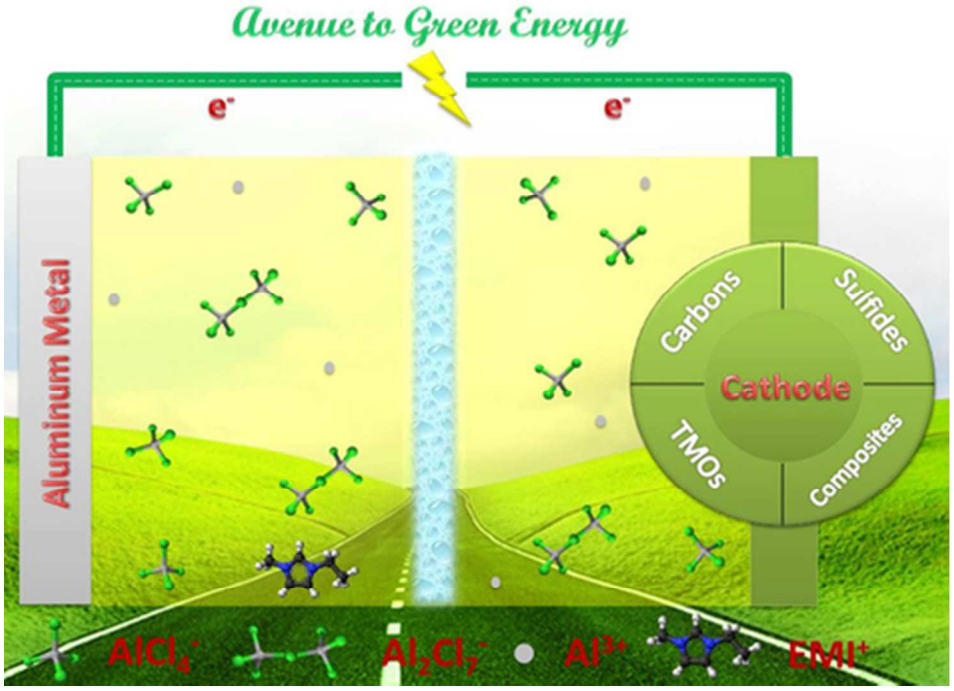

39x29mm (300 x 300 DPI)